ORIGINAL PAPER

Brazing of CoCrFeNi and CoCrFeMnNi equiatomic alloys using 70Au-8Pd-22Ni filler foil

Chieh Lin[1] · Ren-Kae Shiue[1] · Shyi-Kaan Wu[1,2] · Jian-Yuan Huang[1] · Yung-Chien Huang[1]

Abstract

Brazing of CoCrFeNi and CoCrFeMnNi equiatomic alloys using 70Au-8Pd-22Ni (AuPdNi) filler foil by infrared and traditional furnaces was investigated. The wettability of AuPdNi filler on both CoCrFeNi and CoCrFeMnNi substrates is excellent at 1050 °C. CoCrFeNi/AuPdNi/CoCrFeNi joints brazed using infrared and traditional furnaces are composed of Au/Ni-rich solid solutions of different sizes. CoCrFeMnNi/AuPdNi/CoCrFeMnNi joints brazed with an infrared furnace are composed of large globular CoCrFeNi/Ni-rich particles in AuMn intermetallic matrix. In traditional furnace brazed CoCrFeMnNi/AuPdNi/CoCrFeMnNi joints, the AuMn intermetallic compound is uniformly distributed in CoCrFeNi-based and Ni-rich phases. The average shear strengths of both infrared and traditional furnace brazed CoCrFeNi/AuPdNi/CoCrFeNi joints exceed 300 MPa, and all joints fractured at the brazed zone present dimple dominated fracture. In contrast, the traditional furnace brazed CoCrFeMnNi/AuPdNi/CoCrFeMnNi joint has a much lower average shear strength of 173 MPa because of the existence of many solidification shrinkage voids in the brazed zone.

Keywords Brazing · Au-based filler · High-entropy alloy · Microstructure

Introduction

High-entropy alloys (HEAs) have been reported by Yeh et al. as alloys containing at least five elements as the major ingredients, with every element in amounts of 5–35 at% [1, 2]. Numerous researches have demonstrated that HEAs have many outstanding properties due to high entropy, sluggish diffusion, severe lattice distortion, and cocktail effects [2, 3]. The equiatomic CoCrFeMnNi alloy, one of the most popular HEAs, was originally unveiled by Cantor [4]. It has an FCC (face-centered cubic) structure with a single phase below the melting point [5, 6]. The mechanical properties of this HEA are featured with excellent ductility and fracture toughness below room temperatures [7–10]. The CoCrFeMnNi HEA without Mn, i.e., CoCrFeNi equiatomic alloy, also exhibits an FCC structure and has been reported to have mechanical

properties similar to those of CoCrFeMnNi HEA [11, 12]. It has been reported that CoCrFeMnNi forms a face-centered cubic solid solution with exceptional damage tolerance and fracture toughness, especially at low temperatures [7]. It shows potential in a cryogenic application.

Brazing is a joining technique wherein a filler metal is used to join two substrates without melting them. Brazing is suitable for a few applications, which are not appropriate in welding. For instance, a corrosion-resistant plate heat exchanger preferentially manufactured by brazing. Minimum distortion of the plate heat exchanger is achieved because hundreds of brazed joints are simultaneously formed. In contrast, sequential welding may result in huge distortion of the workpiece, so the welding process is seldom used in mass production of the plate heat exchangers. The heating rate in traditional furnace brazing is approximately 0.01–0.2 °C/s, which is greatly slower than that of infrared brazing [13, 14]. The filler melt reacts quickly with the base metal during brazing. Therefore, the early stage of reaction between the molten braze and base metal cannot be examined precisely by using a traditional furnace. Infrared brazing, on the other hand, is featured with a high heating rate up to 50 °C/s and allows accurate temperature control [13, 14]. With the assistance of infrared heating, the initial interfacial reaction can be

✉ Shyi-Kaan Wu
skw@ntu.edu.tw

[1] Department of Materials Science and Engineering, National Taiwan University, Taipei 106, Taiwan

[2] Department of Mechanical Engineering, National Taiwan University, Taipei 106, Taiwan

Table 1 Brazing conditions in the test

Substrate	Brazing temperature (°C)	Furnace type	Brazing time (s)	Specimens
CoCrFeNi	1050	Infrared	300	S/M/W
		Traditional	600	S/M
CoCrFeMnNi	1050	Infrared	300	S/M/W
		Traditional	600	S/M

S, shear test; *M*, metallographic observation; *W*, dynamic wetting angle measurement

evaluated, and the mechanism at the initial stage in brazing can thereby be unveiled. Experimental results have indicated that infrared brazing can be used to examine the microstructural evolution and reaction kinetics of similar/dissimilar brazed joints.

In a previous study, non-equiatomic NiMnFeCoCu HEA was used as a filler metal to braze Inconel 718 superalloy and showed good mechanical performance [15]. However, no studies have reported the use of filler metal to braze HEA. Alloys with high chromium content, such as 316L stainless steel and many nickel-based superalloys, form a protective oxide layer on their surfaces which isolate the substrate from oxidation, but the oxide layer keeps the Ag-based filler metals from wetting the substrate [16–18]. To avoid this problem, a Au-based filler foil has been applied to braze 316L, Inconel 600, and Inconel 718 with quite good results [19–21]. Therefore, the gold-based 70Au-8Pd-22Ni alloy is considered a potential filler metal for brazing CoCrFeMnNi HEA and its derivative CoCrFeNi alloy. In this study, both infrared and traditional furnaces were applied to braze CoCrFeNi and CoCrFeMnNi substrates using 70Au-8Pd-22Ni filler foil. Extensive evaluations of brazed joints have been performed in the experiment.

Experimental

Sample preparation

Equiatomic CoCrFeNi and CoCrFeMnNi ingots of approximately 100 g were prepared with high purity Co, Cr, Fe, Ni, and the master alloy of Ni-Mn in 50–50 in wt%. Ni-Mn master alloy with 99.9 wt% in purity was purchased from Testbourne Ltd., (Hampshire, England, UK) and used to reduce the evaporation of manganese during arc remelting. The purities of the other raw metals were higher than 99.9 wt%. The ingots were remelted 6 times in VAR (vacuum arc remelter) under high purity Ar protection and subsequently homogenized at 1200 °C for 24 h.

The ingots were then cold rolled into plates of 3.5 mm in thickness at room temperature. Specimens with the dimension of $5 \times 7 \times 3.5$ mm^3 for microstructural inspection, wetting angle measurements, and shear tests were cut from the cold-rolled plates. The brazing surfaces of the specimens were ground with SiC papers up to 1200 grit. The 70Au-8Pd-22Ni (in wt%) foil of 50-μm thickness was purchased from Wesgo Company (Hayward, California, USA). The Liquidus temperature of the foil is 1045 °C.

Wetting angle

The dynamic wetting angles of the molten filler metal on both CoCrFeNi and CoCrFeMnNi substrates were measured by the sessile drop test. For this test, 70Au-8Pd-22Ni filler balls of approximately 0.15 g were prepared by VAR. Diagrams of the wetting angle measurement facility, including the specimen holder, can be obtained in previous literature [14, 22]. An ULVAC SINKU-RIKO infrared furnace with a vacuum of 5×10^{-5} mbar was used for dynamic wetting angle measurement. The 70Au-8Pd-22Ni ball was placed on CoCrFeNi and CoCrFeMnNi substrates, respectively. The test conditions used in the dynamic wetting angle measurements were 1050 °C for 300 s, as listed in Table 1.
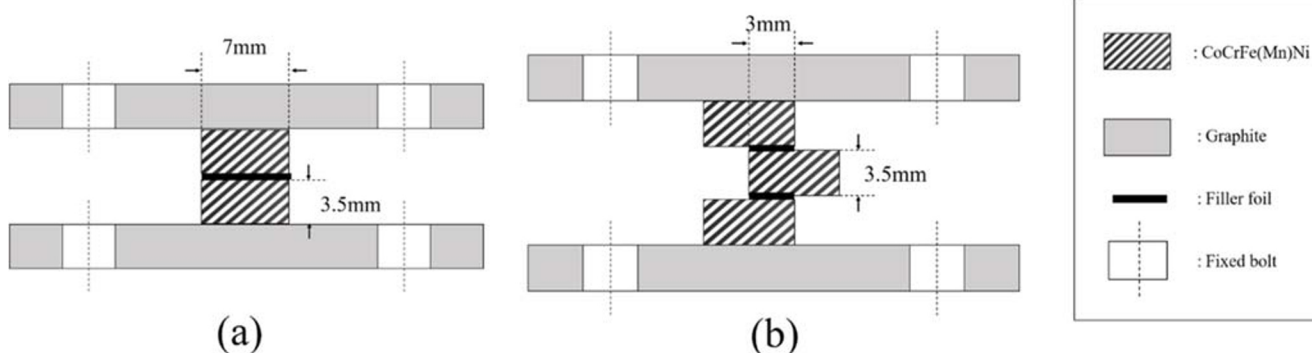
Fig. 1 Schematic diagrams of brazed specimens used for **a** microstructural observation and **b** shear test [14, 22]

Fig. 2 Dynamic wetting angle measurements of AuPdNi filler metal on the CoCrFeNi and CoCrFeMnNi substrates at 1050 °C
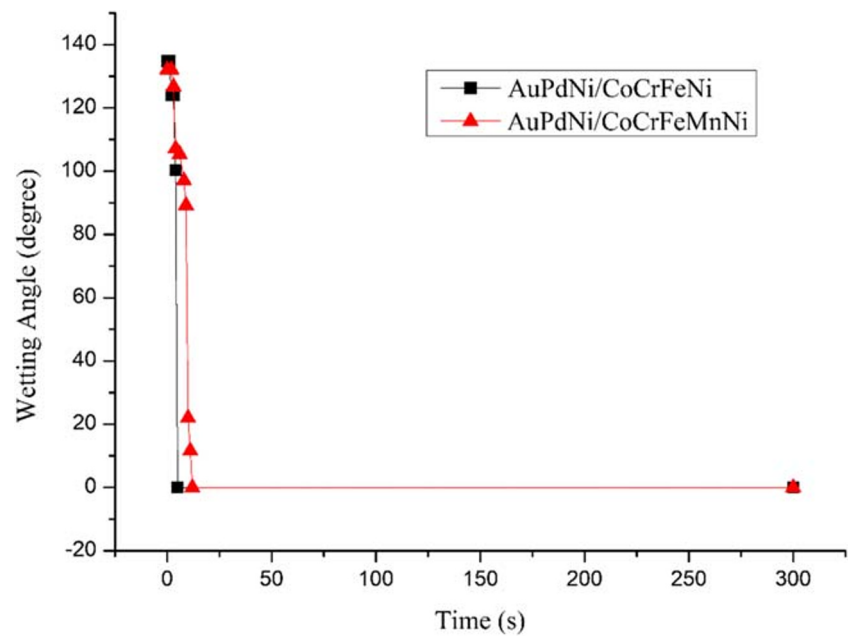
Brazing

The aforementioned infrared furnace with a heating rate of 15 °C/s and a traditional furnace with a heating rate of 0.33 °C/s were used to braze CoCrFeNi and CoCrFeMnNi alloys for microstructural observations and shear tests. During the brazing process, a vacuum of 5×10^{-5} mbar was kept in the furnace. Specimens were preheated at 900 °C for 300 s. The brazing conditions for the microstructural observation and shear test are shown in Table 1. Figure 1a and b present schematic diagrams of specimens enclosed in graphite fixtures for microstructural observations and shear tests, respectively.

Characterization

Quantitative chemical analyses of selected joints were conducted with a JEOL JXA-8200 electron probe microanalyzer (EPMA). Shear tests were performed with a Shimadzu AG-IS universal tensile test machine at a fixed compressive

crosshead speed of 0.0167 mm/s. For each brazing condition, three brazed specimens were evaluated in order to obtain the standard deviation of shear strength. The fractured surfaces and cross sections of the shear test specimens were examined with a NOVA NANO 450 field emission scanning electron microscope (FESEM). Selected fracture surfaces were examined with a Rigaku TTRAX III monochromatized X-ray diffractometer (XRD) for structural analyses.

Results and discussion

Dynamic wetting angle measurement

Figure 2 illustrates dynamic wetting angle measurements of 70Au-8Pd-22Ni filler metal heated at 1050 °C on CoCrFeNi and CoCrFeMnNi substrates. For the CoCrFeNi substrate, the wetting angle is 135° at first. It drops to 100° at 4 s and then to 0° at 5 s. For the CoCrFeMnNi substrate, the wetting angle is 132° in the beginning, rapidly drops to 89° at 9 s, and then

Fig. 3 FESEM BEI cross sections of CoCrFeNi/AuPdNi/CoCrFeNi joints: **a** infrared brazed at 1050 °C for 300 s and **b** traditional furnace brazed at 1050 °C for 600 s
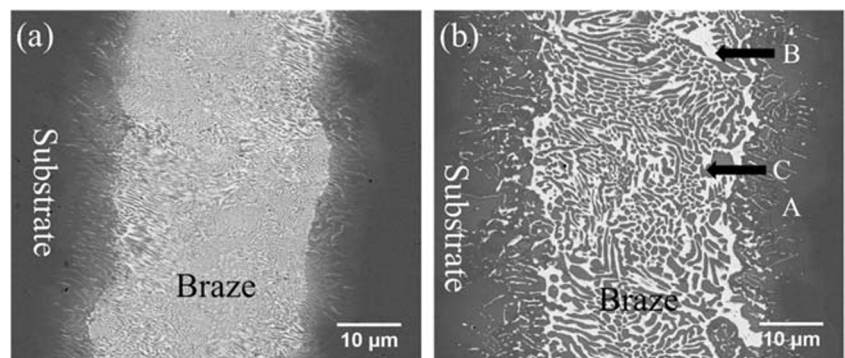
at%	A	B	C
Co	25.6	2.4	15.8
Cr	25.6	12.4	10.4
Fe	24.7	7.0	14.5
Ni	24.1	14.7	51.0
Au	-	53.5	5.9
Pd	-	10.0	2.4
Phase	CoCrFeNi	Au rich	Ni rich

decreases to 0° after 12 s. The dynamic wetting angle is related to the surface tension of molten metal on a substrate. It is obvious that the oxide layers on the two substrates have no effect on the wettability of the 70Au-8Pd-22Ni filler metal. The Au-based filler metal shows excellent wettability on both substrates.

Microstructural observations of CoCrFeNi/AuPdNi/CoCrFeNi joints

Figure 3a, b and Table 2 illustrate the cross sections of FESEM backscattered electron images (BEIs) and the WDS quantitative chemical analysis results of CoCrFeNi/AuPdNi/CoCrFeNi joints infrared brazing at 1050 °C for 300 s and traditional furnace brazing at 1050 °C for 600 s, respectively. The widths of the brazed joints in Figs. 3a and b are 43 μm and 50 μm, respectively. The brazed joints consist of two phases with different sizes, as shown by comparing Fig. 3a and b. The microstructure of the joint in Fig. 3a is much finer than that of the traditional furnace brazed one shown in Fig. 3b due to the

faster cooling cycle of infrared brazing. The slower cooling rate and longer brazing time in traditional furnace brazing result in enhanced diffusion of all ingredients in the brazed zone, leading to the coarsening of the white Au-rich and dark Ni-rich solid solutions (Fig. 3b).

Because the microstructure shown in Fig. 3a is too small to be identified by WDS quantitative chemical analysis, chemical analyses are conducted to examine selected phases in the traditional brazed joint in Fig. 3b. The EPMA analyses are illustrated in Fig. 3b and Table 2. The substrate marked A is CoCrFeNi equiatomic alloy, and no Au and Pd dissolved into the substrate. In the brazed zone, the bright phase marked B is an Au-rich phase, and the dark phase marked C is a Ni-rich phase. The Au/Ni-rich phases are alloyed with Co, Cr, and Fe, indicating that Co, Cr, and Fe in CoCrFeNi substrate dissolve into the Au-rich molten braze in brazing. In contrast, limited solid-state diffusion of Au and Pd from the molten braze into the CoCrFeNi is observed in brazing. According to the binary Au-Ni diagram shown in Fig. 4, solid solution of (Au, Ni) is observed above 810.3 °C [23]. However, it is prone to separate into Au-rich and Ni-rich solid solutions as the temperature decreases below 810.3 °C. This separation agrees with Fig. 3b and Table 2. Joints in Fig. 3a and b are both composed of Au-rich and Ni-rich solid solutions, which are not miscible to each other upon cooling below 810.3 °C. The brazed joint contains no brittle intermetallics, so a ductile joint could be formed (Fig. 4).

Microstructural observation of CoCrFeMnNi/AuPdNi/CoCrFeMnNi joints

Figure 5a, b and Table 3 show FESEM BEIs and quantitative chemical analyses of CoCrFeMnNi/AuPdNi/

Fig. 4 Au-Ni binary alloy phase diagram [23]
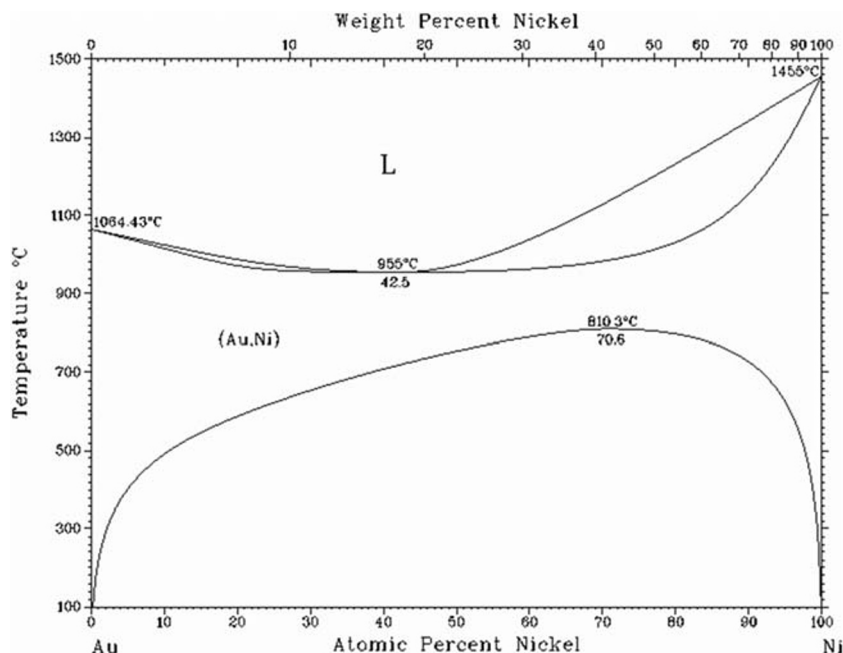
Fig. 5 FESEM BEI cross sections of CoCrFeMnNi/AuPdNi/CoCrFeMnNi joints: **a** infrared brazed at 1050 °C for 300 s and **b** traditional furnace brazed at 1050 °C for 600 s
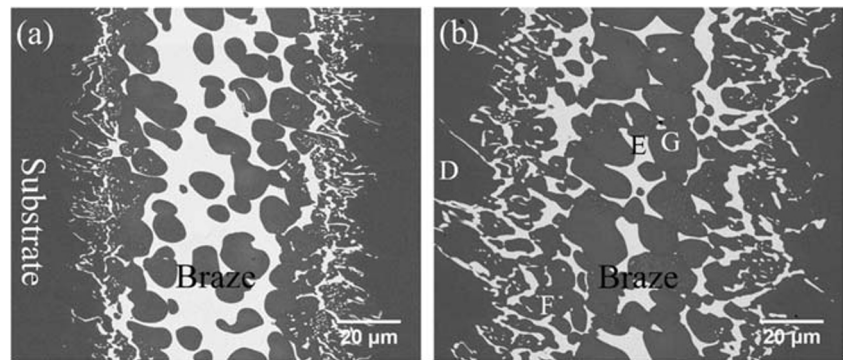
CoCrFeMnNi joints infrared brazing at 1050 °C for 300 s and traditional furnace brazing at 1050 °C for 600 s, respectively. In Fig. 5a, the width of the joint is 90 μm, and the brazed joint includes at least two major phases, as well as a globular dark phase dispersed in the white matrix. In Fig. 5b, the width of the joint is approximately 115 μm, and it is comprised of a dark phase and a white phase. The white phase is uniformly dispersed in the brazed joint. According to the WDS quantitative chemical analyses, the substrate far away from the brazed joint has a composition of approximately equiatomic Co, Cr, Fe, Mn, and Ni. In contrast, the substrate near the brazed zone has higher Ni and lower Mn contents marked D in Fig. 5b. It is obvious that the Mn in the substrate readily dissolves into the braze melt. According to the Au-Mn diagram in Fig. 6, the stoichiometric ratio between Au and Mn in the white phase (marked E in Fig. 5b) is close to that of AuMn intermetallic compound alloyed with minor Co, Cr, Fe, Ni, and Pd [24].

Carefully examining Fig. 5b, one can find two types of dark phase. One is rich and the other is lean in Ni content. The dark area near the interfacial region marked F has the composition of the CoCrFeNi-based phase, in which the Ni content increases but the Mn content decreases significantly as the distance from the substrate increases. The large dark area in the central brazed joint marked G has the composition of Ni-rich phase with Ni content of about 50 at%, but those of

Co, Cr, and Fe are much lower than the composition of CoCrFeNi equiatomic alloy. From the substrate to the central brazed joint, the dark phases are CoCrFeMnNi-based phase marked D, CoCrFeNi-based phase marked F, and then the Ni-rich phase marked G. It is noted that the Mn content is significantly lower in the G phase than in the CoCrFeMnNi substrate due to the consumption of Mn in forming the AuMn intermetallic compound in the brazed zone.
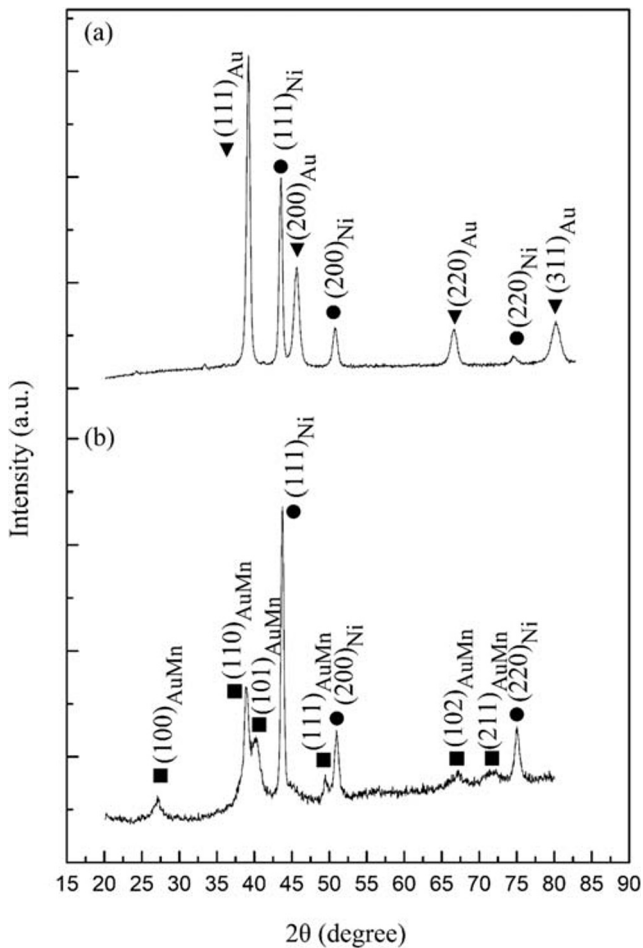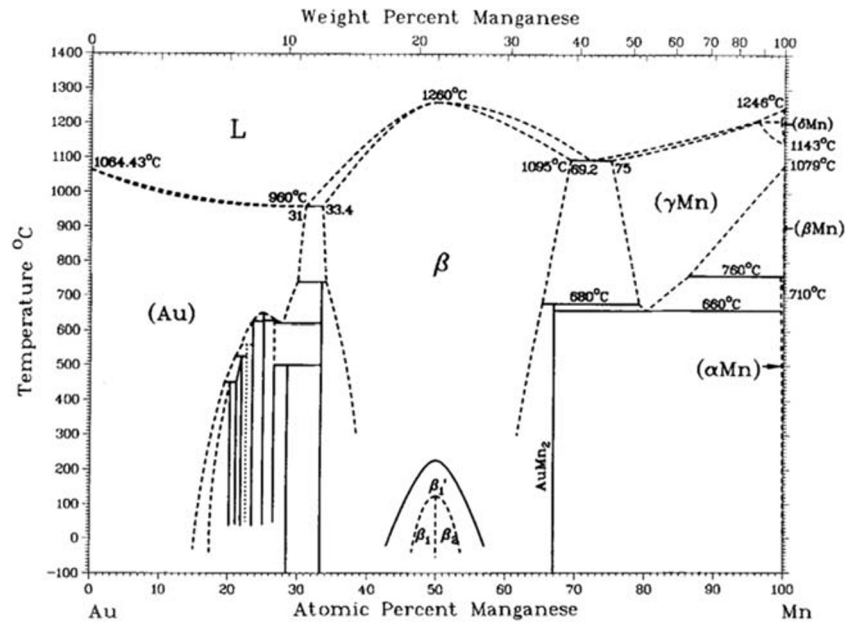
XRD structural analyses of brazed joints

Figure 7a and b display XRD analyses of the fractured surfaces after shear tests of CoCrFeNi/AuPdNi/CoCrFeNi and CoCrFeMnNi/AuPdNi/CoCrFeMnNi joints traditional furnace brazing at 1050 °C for 600 s. From Fig. 7a, two sets of FCC XRD peaks are identified. One is the Ni-rich solid solution and the other is the Au-rich solid solution [25]. Both substrates, CoCrFeNi and CoCrFeMnNi, are not observed in the XRD analyses, because cracks were initiated and propagated along the brazed zone. From Fig. 7b, the XRD peaks of AuMn intermetallic phase and Ni-rich solid solution are identified. The AuMn intermetallic compound has a tetragonal structure with lattice constants of 0.32706 nm and 0.31659 nm [24]. From these lattice parameters, the corresponding (hkl) plane for each X-Ray peak shown in Fig. 7b is identified. Both XRD structure analyses are consistent with the aforementioned WDS chemical analyses.

Table 3 EPMA chemical analyses in Fig. 5b

at%	Base metal	D	E	F	G
Co	20.2	21.9	0.4	23.1	15.4
Cr	20.5	22.0	1.6	20.0	15.3
Fe	20.0	22.0	0.6	20.9	15.6
Mn	19.8	9.4	41.8	3.9	3.4
Ni	19.5	24.2	3.5	30.9	47.9
Au	-	0.4	43.4	0.8	1.6
Pd	-	0.2	8.7	0.4	0.8
Phase	HEA	CoCrFeMnNi based	AuMn	CoCrFeNi based	Ni rich

Fig. 6 Au-Mn binary alloy phase diagram [23]

Fig. 7 XRD structural analyses of the fractured surfaces after shear tests: **a** CoCrFeNi/AuPdNi/CoCrFeNi and **b** CoCrFeMnNi/AuPdNi/ CoCrFeMnNi joints traditional furnace brazed at 1050 °C for 600 s

Table 4 displays the average shear strengths of joints brazed under various conditions. Average shear strengths of CoCrFeNi/AuPdNi/CoCrFeNi joints brazing at 1050 °C for 300 s in an infrared furnace and at 1050 °C for 600 s in a traditional furnace are 340 MPa and 365 MPa, respectively. The size of the immiscible Au-rich and Ni-rich phases has little effect on the joint shear strengths. Figure 8a, b, c, and d show BEI cross sections and SEI fractographs of specimens infrared brazing at 1050 °C for 300 s, and specimens traditional furnace brazing at 1050 °C for 600 s, respectively. Based on Fig. 8, both brazed joints fracture at the brazed zone and the SEI fractographs indicate ductile dimple fracture. The size of dimples in the infrared brazed joint (Fig. 8b) is much smaller than that of traditional brazed one (Fig. 8d). It is consistent with the microstructural observations illustrated in Fig. 3. Additionally, the presence of Au/Ni-rich solid solutions with FCC structure increases the ductility of the brazed joints. The 70Au-8Pd-22Ni filler foil demonstrates great potential for brazing CoCrFeNi equiatomic alloy.

Table 4 lists the average shear strengths of the CoCrFeMnNi/AuPdNi/CoCrFeMnNi joints brazing at 1050 °C for 300 s and traditional furnace brazing at 1050 °C for 600 s, which are 326 MPa and 173 MPa, respectively. A huge decrease in average shear strength is obtained in the traditional furnace brazed joint. Figure 9a and b show a BEI cross section and an SEI fractograph of the joint infrared brazing at 1050 °C for 300 s. According to Fig. 9a, the crack propagates along with the white AuMn intermetallic phase, as pointed by

Table 4 Average shear strength of brazed joints

Substrate	Brazing temperature (°C)	Furnace type	Brazing time (s)	Average shear strength (MPa)
CoCrFeNi	1050	Infrared	300	340 ± 17
		Traditional	600	365 ± 9
CoCrFeMnNi	1050	Infrared	300	326 ± 6
		Traditional	600	173 ± 43

the arrow. Additionally, the globular dark Ni-rich solid solution undergoes severe plastic deformation. Thus, the SEI fractograph in Fig. 9b presents a cleavage-dominated fracture.

Figure 9c and d show a BEI cross section and an SEI fractograph of the joint traditional furnace brazing at 1050 °C for 600 s. As can be seen in Fig. 9c, the joint fractures at the interface between the brazed zone and CoCrFeMnNi substrate. It is noted that isothermal solidification shrinkage voids with dendritic morphology are visible in the FESEM SEI fractograph in Fig. 9d. The shrinkage voids are commonly observed in laser welding of cast and rolled HEAs for low-temperature applications in previous study [26]. According to the experimental result, the mechanism to produce the shrinkage voids is the same between welding and brazing. The presence of many isothermal solidification shrinkage voids significantly impairs the average shear strength of the traditional furnace brazed one.

The amount of the CoCrFeMnNi dissolved into the molten braze is enhanced in the traditional furnace brazed joint due to its slower brazing cycle. In addition, the dissolution of CoCrFeMnNi into the Au-rich braze melt could result in isothermal solidification during brazing. Many solidification shrinkage voids are found in the fractograph of the traditional furnace brazed joint. However, the amount of solidification shrinkage voids in the brazed zone can be inhibited by using infrared heating, which is characterized by a much faster thermal history.

Conclusions

Wettability, microstructural evolution, and shear tests of CoCrFeNi and CoCrFeMnNi equiatomic alloys brazed in infrared and traditional furnaces with 70Au-8Pd-22Ni filler foil have been investigated. The important results are summarized below.

Fig. 8 FESEM observations of the fractured braze joints after the shear test: **a** BEI cross section, **b** SEI fractograph of CoCrFeNi/AuPdNi/CoCrFeNi joint infrared brazed at 1050 °C for 300 s, **c** BEI cross section, and **d** SEI fractograph of CoCrFeNi/AuPdNi/CoCrFeNi joint traditional furnace brazed at 1050 °C for 600 s
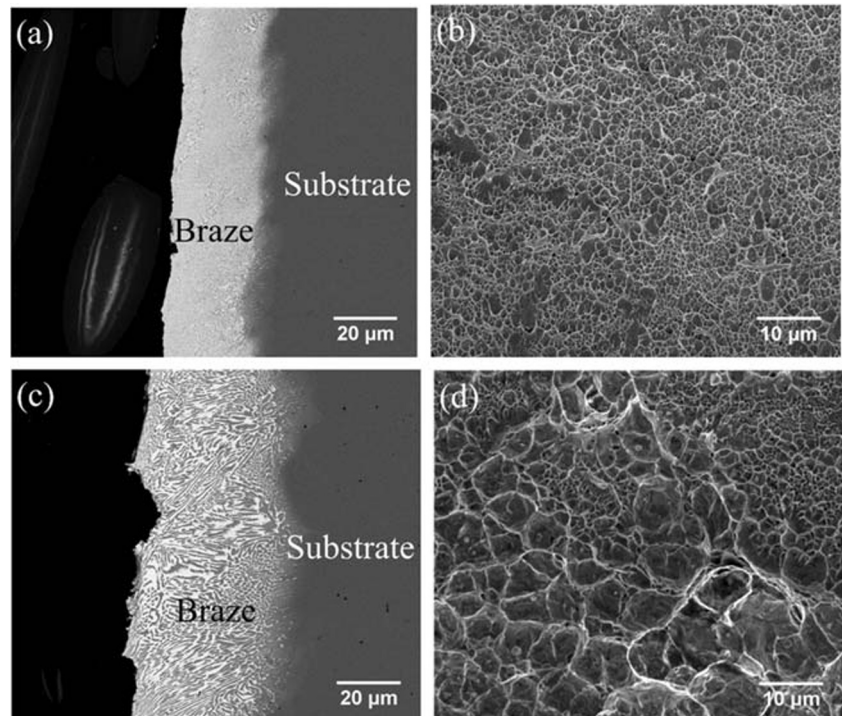
Fig. 9 FESEM observations of the fractured braze joints after the shear test: **a** BEI cross-section, **b** SEI fractograph of CoCrFeMnNi/ AuPdNi/CoCrFeMnNi joint infrared brazed at 1050 °C for 300 s, **c** BEI cross-section, and **d** SEI fractograph of CoCrFeMnNi/ AuPdNi/CoCrFeMnNi joint traditional furnace brazed at 1050 °C for 600 s
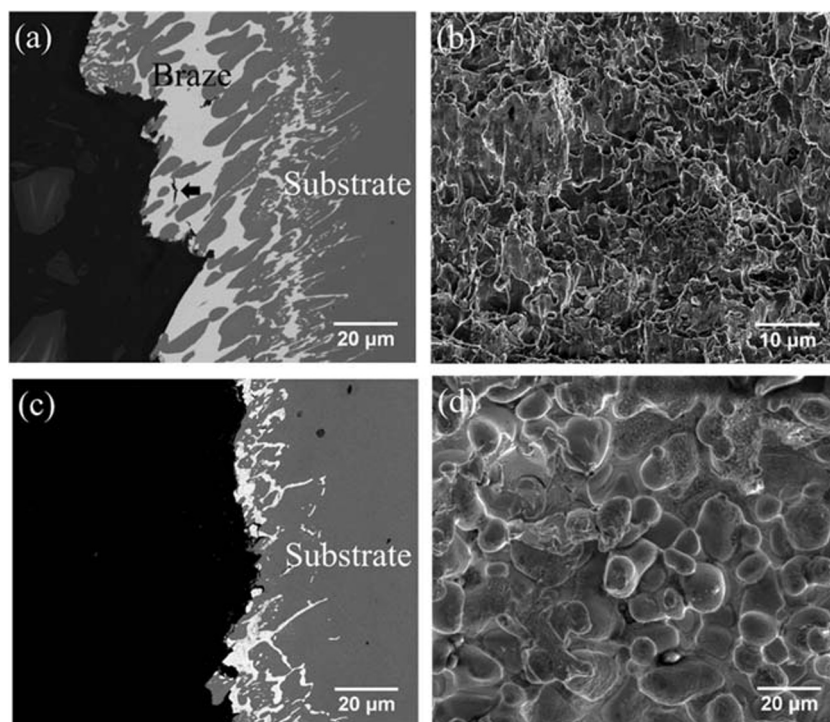
1. Dynamic wetting angle measurements indicate that the wettability of 70Au-8Pd-22Ni filler metal on CoCrFeNi and CoCrFeMnNi substrates is excellent at 1050 °C.
2. CoCrFeNi/AuPdNi/CoCrFeNi joints brazed with both infrared and traditional furnaces are composed of Au-rich and Ni-rich solid solutions with different grain sizes. The mixture of Au-rich and Ni-rich solid solutions coarsens in the traditional furnace brazing due to the slower thermal history of the brazing. The average shear strengths of the CoCrFeNi/AuPdNi/CoCrFeNi joints exceeds 300 MPa, and the fractograph indicates dimple dominated fracture.
3. The infrared brazed CoCrFeMnNi/AuPdNi/ CoCrFeMnNi joints are composed of large CoCrFeNi/ Ni-rich particles in the AuMn intermetallic matrix. By contrast, in the traditional brazed joints, the AuMn intermetallic compound is uniformly mixed with the CoCrFeNi-based and Ni-rich solid solutions because of the enhanced dissolution of CoCrFeMnNi base metal into the Au-rich melt during brazing. The average shear strength of infrared brazed CoCrFeMnNi/AuPdNi/ CoCrFeMnNi joint is 326 MPa, and the fractograph shows quasi-cleavage-dominated fracture. In contrast, the traditional furnace brazed joint has a much lower average shear strength of 173 MPa, because many solidification shrinkage voids are formed in the brazed zone.

Compliance with ethical standards

Conflict of interest   The authors declare that they have no conflict of interest.

References

1. Yeh JW, Chen SK, Lin SJ, Gan JY, Chin TS, Shun TT, Tsau CH, Chang SY (2004) Nanostructured high-entropy alloys with multiple principal elements: novel alloy design concepts and outcomes. Adv Eng Mater 6(5):299–303. https://doi.org/10.1002/adem.200300567
2. Yeh JW (2006) Recent progress in high-entropy alloys. Ann Chim Sci Mater 31(6):633–648
3. Yeh JW (2013) Alloy design strategies and future trends in high-entropy alloys. JOM 65(12):1759–1771. https://doi.org/10.1007/s11837-013-0761-6
4. Cantor B, Chang ITH, Knight P, Vincent AJB (2004) Microstructural development in equiatomic multicomponent alloys. Mater Sci Eng A 375-377:213–218. https://doi.org/10.1016/j.msea.2003.10.257
5. Otto F, Yang Y, Bei H, George EP (2013) Relative effects of enthalpy and entropy on the phase stability of equiatomic high-entropy alloys. Acta Mater 61(7):2628–2638. https://doi.org/10.1016/j.actamat.2013.01.042
6. Tsai KY, Tsai MH, Yeh JW (2013) Sluggish diffusion in Co–Cr–Fe–Mn–Ni high-entropy alloys. Acta Mater 61(13):4887–4897. https://doi.org/10.1016/j.actamat.2013.04.058
7. Gludovatz B, Hohenwarter A, Catoor D, Chang EH, George EP, Ritchie RO (2014) A fracture-resistant high-entropy alloy for cryogenic applications. Science 345(6201):1153–1158. https://doi.org/10.1126/science.1254581
8. Otto F, Dlouhý A, Somsen C, Bei H, Eggeler G, George EP (2013) The influences of temperature and microstructure on the tensile

properties of a CoCrFeMnNi high-entropy alloy. Acta Mater 61(15):5743–5755. https://doi.org/10.1016/j.actamat.2013.06.018

9. Gludovatz B, George EP, Ritchie RO (2015) Processing, microstructure and mechanical properties of the CrMnFeCoNi high-entropy alloy. JOM 67(10):2262–2270. https://doi.org/10.1007/s11837-015-1589-z

10. Gali A, George EP (2013) Tensile properties of high- and medium-entropy alloys. Intermetallics 39:74–78. https://doi.org/10.1016/j.intermet.2013.03.018

11. Wu Z, Bei H, Otto F, Pharr GM, George EP (2014) Recovery, recrystallization, grain growth and phase stability of a family of FCC-structured multi-component equiatomic solid solution alloys. Intermetallics 46:131–140. https://doi.org/10.1016/j.intermet.2013.10.024

12. Wu Z, Bei H, Pharr GM, George EP (2014) Temperature dependence of the mechanical properties of equiatomic solid solution alloys with face-centered cubic crystal structures. Acta Mater 81: 428–441. https://doi.org/10.1016/j.actamat.2014.08.026

13. Lee SJ, Wu SK, Lin RY (1998) Infrared joining of TiAl intermetallics using Ti—15Cu—15Ni foil—I. The microstructure morphologies of joint interfaces. Acta Mater 46(4):1283–1295. https://doi.org/10.1016/S1359-6454(97)00298-X

14. Shiue RK, Wu SK, Chen SY (2003) Infrared brazing of TiAl intermetallic using BAg-8 braze alloy. Acta Mater 51(7):1991–2004

15. Bridges D, Zhang S, Lang S, Gao M, Yu Z, Feng Z, Hu A (2018) Laser brazing of a nickel-based superalloy using a Ni-Mn-Fe-Co-Cu high entropy alloy filler metal. Mater Lett 215:11–14. https://doi.org/10.1016/j.matlet.2017.12.003

16. Montemor MF, Ferreira MGS, Hakiki NE, Da Cunha BM (2000) Chemical composition and electronic structure of the oxide films formed on 316L stainless steel and nickel based alloys in high temperature aqueous environments. Corros Sci 42(9):1635–1650. https://doi.org/10.1016/S0010-938X(00)00012-3

17. Kozlova O, Voytovych R, Devismes MF, Eustathopoulos N (2008) Wetting and brazing of stainless steels by copper–silver eutectic.

18. Shiue RK, Chen CP, Wu SK (2015) Infrared brazing of $Ti_{50}Ni_{50}$ shape memory alloy and 316L stainless steel with two sliver-based fillers. Metall Mater Trans A 46(6):2364–2371. https://doi.org/10.1007/s11661-015-2830-7

19. Shiue RK, Wu SK, Chen CP, Yang SH (2015) Infrared brazing of $Ti_{50}Ni_{50}$ shape memory alloy and 316L stainless steel with Au-22Ni-8Pd filler. Gold Bull 48(1–2):57–62. https://doi.org/10.1007/s13404-015-0160-6

20. Schwartz MM (1975) Applications for gold-base brazing alloys. Gold Bull 8(4):102–110. https://doi.org/10.1007/BF03215078

21. Shiue RK, Wu SK, Liu CK, Dai CY (2017) Interfacial reaction and bonding strength of $Ti_{50}Ni_{50}$ and Inconel 600 dissimilar brazed joints. Mater Trans 58(9):1308–1312. https://doi.org/10.2320/matertrans.M2017123

22. Shiue RH, Wu SK (2006) Infrared brazing of $Ti_{50}Ni_{50}$ shape memory alloy using two Ag–Cu–Ti active braze alloys. Intermetallics 14(6):630–638. https://doi.org/10.1016/j.intermet.2005.10.012

23. Massalski TB, Murray JL, Bennett LH, Baker H (1986) Binary alloy phase diagrams. American Society for Metals, Metals Park

24. American Society for Metals, United States. National Bureau of Standards (1985) Bulletin of alloy phase diagrams, vol 6. American Society for Metals, Metals Park

25. Swanson HE, United S, National Bureau of S (1953) Standard X-ray diffraction powder patterns. U.S. Dept. of Commerce, National Bureau of Standards: For sale by the Supt. of Docs., U.S. G.P.O., Washington, DC

26. Nam H, Park C, Moon J, Na Y, Kim H, Kang N (2019) Laser weldability of cast and rolled high-entropy alloys for cryogenic applications. Mater Sci Eng A 742:224–230. https://doi.org/10.1016/j.msea.2018.11.009

Mater Sci Eng A 495(1):96–101. https://doi.org/10.1016/j.msea.2007.10.101